Optical Materials 104 (2020) 109844

Contents lists available at ScienceDirect

Optical Materials

journal homepage: http://www.elsevier.com/locate/optmat

Synergistic effects of sodium fluoride (NaF) on the crystallinity and band gap of Fe-doped TiO_2 developed via microwave-assisted hydrothermal treatment

Majid Jahdi [a,**], Shivani B. Mishra [a], Edward N. Nxumalo [a], Sabelo D. Mhlanga [b], Ajay K. Mishra [a,*]

[a] Nanotechnology and Water Sustainability Research Unit, College of Science, Engineering and Technology, University of South Africa, Florida, 1709, Johannesburg, South Africa

[b] DST/Mintek Nanotechnology Innovation Centre, Council for Mineral Technology (MINTEK), Private Bag X3015, Randburg, 2125, South Africa

ARTICLE INFO

Keywords:
Nanocomposite
Titanium dioxide
Iron
Photocatalytic
Hydrothermal

ABSTRACT

Titanium dioxide-based nanocomposite materials are the most widely used materials to enhance the photocatalytic activity of titanium dioxide (TiO_2) due to their excellent light absorbing properties. However, the wide use of TiO_2 is restricted by its large band gap. Doping TiO_2 with iron (Fe) is one of the strategies that have been employed in order to narrow the band gap of TiO_2, thus promoting its photocatalytic activity to the visible light region. In this work, new energy levels between the valence band and the conduction band were introduced by incorporating Fe in the TiO_2 lattice resulting to an effective shift of the light absorption to the visible light region. On the other hand, the incorporation of NaF in the TiO_2 lattice led to significant changes on its crystal phases from brookite-anatase to anatase-rutile phases. In this study, the hydrothermal synthesis route was combined with microwave heating as a smart pathway of reducing the synthesis cost by reducing synthesis temperature and time while achieving an efficient photocatalytic activity of the TiO_2 nano-photocatalysts. XRD diffraction patterns demonstrated that a mixture of brookite-anatase was obtained, which was transformed to the anatase-rutile phases after doping TiO_2 with Fe in the presence of NaF. Microscopic investigations further showed that the doped TiO_2 nano-photocatalyts exhibited a spherical shape with an average particle size in the range of 10–20 nm. UV–Vis analysis showed that the indirect and direct band gap of Fe-doped TiO_2 in the presence of NaF was significantly narrowed to 1.67–1.83 eV and 2.05–2.17 eV, respectively. The synergistic effect of NaF on the crystallinity of Fe-doped TiO_2 calcined at 400 °C in air was demonstrated to form an anatase-rutile phase.

1. Introduction

Titanium dioxide (TiO_2) is considered as a key nano-photocatalyst for use in water treatment applications due to its unique properties, such as, high stability, low cost, relatively low toxicity and excellent absorbing propensity for solar light compared to other semiconductors [1]. However, the photocatalytic activity of TiO_2 is restricted to the ultraviolet (UV) region due to its wide band gap [2]. Generally, TiO_2 naturally exists as a single phase or a mixture of phases of its three polymorphs namely; rutile, anatase, and brookite with a band gap of 3.0, 3.2, and 3.4 eV, respectively [3]. Hence, with these phases, TiO_2 is only sensitive in the UV wavelengths [4]. In fact, the band gap of TiO_2 does not strictly depend on its crystal phase but is also strongly controlled by its morphology and the presence of impurity elements in the oxide lattice [5]. For this, many studies have been initiated to modify TiO_2 band gap in order to target broad light absorption. The incorporation of cationic dopants in the TiO_2 lattice is one of the main pathways to narrow the band gap and then resolve the photocatalytic activity weakness of TiO_2 [6].

Among the different variety of metal ions, Fe^{3+} has been considered as an efficient candidate to modify the TiO_2 lattice owing to its ionic radius of 0.064 nm, which is relatively similar to that of Ti^{4+} (0.068 nm), which facilitates its implantation into the TiO_2 lattice [7]. The incorporation of Fe^{3+} as a Ti^{4+} substitute into the TiO_2 lattice is one of the

* Corresponding author.
** Corresponding author.
E-mail addresses: majid.jahdi@gmail.com (M. Jahdi), mishrak@unisa.ac.za (A.K. Mishra).

https://doi.org/10.1016/j.optmat.2020.109844
Received 17 October 2019; Received in revised form 12 March 2020; Accepted 19 March 2020
Available online 28 March 2020

best pathways to narrow the band gap of TiO_2 due to its excellent properties, including absorption in the visible range of the solar spectrum, high stability, low cost, ready availability, and its optical band gap in the range 2.0–2.2 eV [8]. Moreover, doping TiO_2 with Fe influences the dynamics of electron/hole recombination and interfacial charge transfer. Fe is believed to be an efficient dopant to enhance the photocatalytic efficiency of TiO_2 and has a direct influence on the intrinsic properties of TiO_2 such as adding new energy levels into TiO_2 band gap and enhancing the separation of photo-generated electrons and holes by trapping them temporarily and superficially [9]. Fe also serves to develop a magnetic TiO_2 photocatalyst that can be aggregated rapidly under the influence of a magnetic field resulting to easy separation of the nanoparticles in water treatment applications [10,11].

Fluorine (F) is an exceptional anionic element due to its high electronegativity, thus serving as an electron donor which induces the formation of reduced Ti^{3+} centers that localize the extra electrons needed for charge compensation [12]. It has been widely used as a morphology controlling agent to control the growth of the anatase phase, especially (001) anatase [13]. Unlike Na ion (Na^+), widely used to get oxygen deficiency (TiO_{2-x}), which is an adequate element to synthesize a single rutile phase structure [14,15]. Due to the large ionic radius of Na^+ (~0.102 nm), it cannot substitute Ti^{4+} with radius of 0.068 nm but instead it can migrate to the TiO_2 surface forming Na_2O [16].

Doping TiO_2 with Fe ions in the presence of Na and F is one of the efficient pathways to synthesize TiO_2 with both anatase and rutile phases in order to achieve a significant shift of photocatalytic activity to the visible region [17]. The use of these elements to modify the structure, morphology and band gap of TiO_2 lead to an efficient shifting of the photocatalytic activity to the visible region [18].

The use of the microwave-assisted hydrothermal synthesis method is one of the greener methodologies to synthesize nanocomposites with high performance and within a short time [19]. Microwave-assisted hydrothermal synthesis is an effective method for producing efficient nanocomposites by controlling the particle size through the nucleation and growth kinetics [20,21]. Cui et al. have investigated the microwave-assisted hydrothermal synthesis method to grow TiO_2 nanotubes on Ni foam substrates [22]. Ocakoglu et al. reviewed some aspects and advantages of hydrothermal synthesis assisted microwave heating method. The combination of hydrothermal and microwave heating processes offered an effective approach to significantly reduce the temperature, time, and costs in chemical synthesis [20].

In this study, a fast one-step microwave-assisted hydrothermal synthesis method was employed to synthesize highly efficient NaF/Fe-doped TiO_2 nanocomposites. The main goal was to demonstrate the synergic effect of varying the amount of both Fe and NaF on the band gap of the synthesized TiO_2 nanocomposites and also to study the influence of the coexistence of Na and F ions on the growth of both anatase and rutile phases of TiO_2. The successful synthesis of TiO_2 nanocomposites with much smaller band gap energies using these dopants was an important finding in this work and presented a simplified greener way of making the materials for environmental applications such as the photocatalytic degradation of organics in water.

2. Experimental

2.1. Materials and reagents

Titanium (IV) butoxide purum, ≥97.0% (gravimetric) with density of 1 g/ml was used as TiO_2 source. Iron chloride (reagent grade, with 97% purity) was used as a source of iron. Sodium fluoride (analytical reagent) was used as a source of Na^+ and F^-, and 2-butanol with purity ≥99.5% (gravimetric) was used as a solvent for the mixture [23]. All the reagents were purchased from Merck, South Africa and they were used without any further purification. Deionized water was prepared in our laboratory using a Direct-Q® (Millipore) purification system.

2.2. Preparation of Fe-doped TiO_2 nanocomposites

Briefly, in a glass beaker of 500 ml, 13, 12.2, 11.8, 10.9, 10, 8.7, 8, and 6.7 ml of titanium butoxide ($Ti(OC_4H_9)_4$) corresponding to 100, 90, 89, 82, 75, 65, 60, and 50% of TiO_2, respectively were dissolved in 100 ml of 2-butanol ($CH_3CH(OH)CH_2CH_3$). In separate beakers, 90, 724.3, 1358, 2263, 2716, and 2263 mg of iron chloride ($FeCl_3$) equivalent to 0, 1, 8, 15, 25, and 30% of iron, respectively were dissolved in deionized water, Also in a separate beakers, 311.9 and 779.9 mg of sodium fluoride equivalent to 10 and 25% of NaF respectively, were dissolved in water. $Ti(OC_4H_9)_4$ was dissolved in 2-butanol and $FeCl_3$ was dissolved in deionized water and these were simultaneously added dropwise to the NaF dissolved in water under sonication and mechanical stirring at room temperature. After 30 min, a suspension was formed and stirred under magnetic stirring for 4 h (h) at room temperature.

Subsequently, suspensions formed were transferred into reaction vessels and placed in ultra-strength frame closed reaction vessels. In fact, nanocomposites were synthesized by microwave-assisted hydrothermal synthesis at 180 °C within 1 h using the MDS-6G microwave digestion with power of 220–240 VAC 50/60Hz 8A and microwave frequency of 2450 MHz. The main advantage of this microwave technique is that it is fast, simple, and easy to obtain materials with targeted properties such as nanoscale size, good dispersion, uniform structures and morphology [24].

The nanocomposites were then washed with ethanol to remove any organic impurities using an ultracentrifuge with a speed of 12000 rpm for 1 h30 min, followed by washing with deionized water three times to remove any residual ions remaining in the prepared nanocomposites. Furthermore, the samples were then dried in the oven at 100 °C for 8 h, crushed in a mortar, and calcined in a muffle furnace at 400 °C for 4 h with increasing step of 5 °C per minute in air.

Table 1 presents the designated labels used to name the prepared samples with different amount of Fe and NaF in terms of moles.

2.3. Analysis of Fe doped TiO_2 nanocomposites

X-ray diffraction (XRD) analysis of the materials was done using a PANalytical X'Pert PRO X-Ray Diffractometer. X-ray photoelectron spectrometer (XPS) survey spectrum and high resolution XPS spectra were obtained by using an AXIS SupraTM. The AXIS Supra is a high-performance X-Ray photoelectron spectrophotometer, with unrivalled sensitivity and energy resolution. Moreover, it is an efficient collection of photoelectrons by the magnetic and electrostatic lenses combined with a high transmission energy analyzer. Scanning electron microscopy (SEM) images and energy dispersive spectroscopy (EDS) spectra were obtained using a JEOL-7800F Field Emission Scanning Electron Microscope (FE-SEM) with a cathodololuminescence spectrometer. Prior to HR-SEM analysis, the samples were coated with carbon to increase their conductivity and prevent them from charging. The microstructure of the materials was studied by using a JEOL JEM-2100 transmission electron microscope (TEM). The JEOL JEM-2100 is designed to be an analytical facility to investigate and characterize the internal structure of very thin

Table 1
Designated labels of the TiO_2 nanocomposites with different amounts of Fe and NaF.

Nanocomposite nomenclature	Nanocomposite composition in terms of molar mass
NaF10.TiO_2	TiO_2 in the presence 10% of NaF
NaF10-Fe1TiO_2	1% of Fe doped TiO_2 in the presence 10% of NaF
NaF10-Fe8TiO_2	8% of Fe doped TiO_2 in the presence 10% of NaF
NaF10-Fe15TiO_2	15% of Fe doped TiO_2 in the presence 10% of NaF
NaF10-Fe25TiO_2	25% of Fe doped TiO_2 in the presence 10% of NaF
NaF10-Fe30TiO_2	30% of Fe doped TiO_2 in the presence 10% of NaF
NaF10-FexTiO_2	x % of Fe doped TiO_2 in the presence 10% of NaF
NaF25-Fe25TiO_2	25% of Fe doped TiO_2 in the presence 25% of NaF

sections of material, up to around 200 nm thick depending on the atomic number of the material. By using the Lambda 650 UV/VIS spectrometer over a wavelength range of 250 nm–800 nm, UV–Vis absorbance was measured. The band gap of TiO_2 nanocomposites is derived from the Kubelka-Munk (KM) expression and Tauc equation. Kubelka-Munk (KM) expression is:

$$F(R) = \frac{(1-R)^2}{2R} \quad (1)$$

Where R is the reflectance of the sample.

And the Tauc equation is:

$$(\alpha h\nu)^{1/n} = B(h\nu\text{-}Eg) \quad (2)$$

Where α is the optical absorption coefficient, hν is the incident photon energy in eV, B is material dependent absorption constant, and Eg is the band gap of the material to be determined. Assuming that α is proportional to F(R) which is obtained from reflectance of the sample converted from Kubelka-Munk function; the F(R) substitute α in Tauc equation. Indeed, the band gap can be attained by extrapolation of the straight-line part of the Tauc plot ($(F(R)h\nu)^{1/n}$ versus hν) to intersect with hν (eV) axes.

As well, n represent the constant that depending on the nature of electronic transition.

Where, n = ½ for permitted direct transition of the materials.
n = 2 for permitted indirect transition of the materials [25,26].

3. Result and discussion

3.1. X-ray diffraction (XRD) analysis

The XRD patterns for TiO_2, NaF10-TiO_2, NaF10-FexTiO_2, and NaF25-Fe25TiO_2 are shown in Fig. 1. The XRD patterns of the undoped TiO_2 nanomaterials exhibited diffraction peaks with high intensity at 2θ = 25.35°, 38.04°, 47.90°, 54.47°, and 62.60° corresponding to the (101), (103)/(004)/(112), (200), (105)/(211), and (204) diffraction planes of anatase TiO_2 (JCPDS, file No. 21-1272) [21,27]. Moreover, the characteristic peak of brookite at 2θ = 30.6°, which existed only in the XRD patterns of the undoped TiO_2 and is not superposed with any diffraction peaks of anatase phase was used to prove the presence of brookite TiO_2 (JCPDS card No. 29-1360) [28].

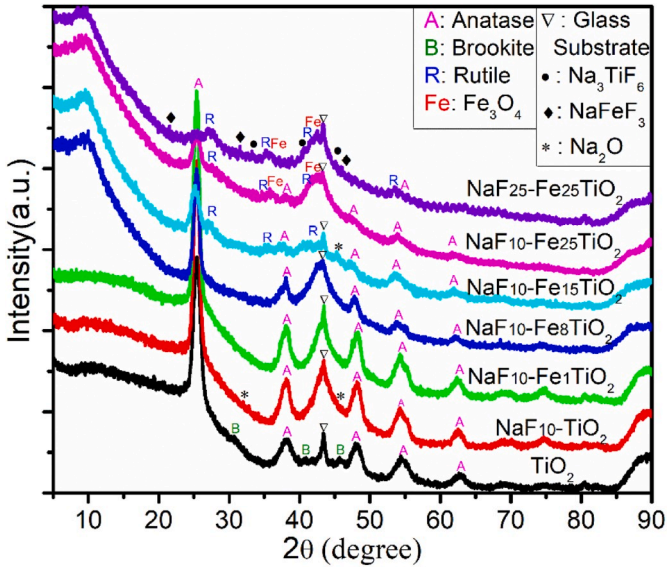

Fig. 1. X-ray diffraction patterns for undoped TiO_2, NaF10-TiO_2, NaF10-FexTiO_2, and NaF25-Fe25TiO_2 calcined at 400 °C.

The XRD patterns of the prepared TiO_2 in the presence of 10% of NaF is similar to that of the undoped TiO_2; the only difference found is the appearance of a wide peak which belongs to Na_2O crystalline phase [29].

On the other XRD patterns, the diffraction peaks of Fe_3O_4 can be indexed using the JCPDS card No. 65-3107 [30,31]. Only, the reflection peaks at 2θ = 35.75° corresponding to (400) diffraction plane of the Fe_3O_4 nanostructure phase indicate the presence of Fe_3O_4 phase, unlike other peaks which were superimposed with the other phases. The XRD patterns of the synthesized NaF25-Fe25TiO_2 nanocomposites showed the anatase diffraction peaks with lower intensities than those of rutile phase which clearly appears when the amount of both Fe and NaF (2θ positions of 27.28°, 35.81°, 41.10°, and 53.96°) were increased. This matched with the rutile TiO_2 phase (JCPDS No. 21-1276) [32,33]. Furthermore, Na_3TiO_6 and $NaFeF_3$ phases appeared when the amount of NaF was increased to 25% in terms of moles [34,35].

Initially, the XRD pattern revealed that the crystallinity of TiO_2 was brookite-anatase phase which was converted to a single anatase phase in the presence of 10% NaF. On the other hand, by keeping the same amount of NaF and increasing the amount of Fe, there was an appearance of the rutile phase which was clearly evident in the XRD pattern of NaF10-Fe15TiO_2. Moreover, the crystallization of NaF10-Fe25TiO_2 and NaF25-Fe25TiO_2 resulted in clearly high conversion of anatase phases into rutile phases. The XRD patterns revealed that the crystallinity of the undoped TiO_2 was only brookite-anatase and the NaF25-Fe25TiO_2 synthesized nanocomposites were composed of TiO_2 anatase, rutile, Na_3TiF_6, $NaFeF_3$, and Fe_3O_4 phases. However, it should be noted that there was no existence of rutile crystalline phase in the undoped TiO_2 and no existence of brookite phase in all other prepared nanocomposites. The peak at 2θ = 43.33°, present in all XRD patterns, belongs to the glass substrate [36].

3.2. X-ray photoelectron spectroscopy (XPS) analysis

The XPS survey spectrum of NaF25-Fe25TiO_2 nanoparticles prepared by the microwave-assisted hydrothermal synthesis method showed the presence of Ti 2p, O 1s, F 1s, Na 1s and Fe 2p (Fig. 2a). The high resolution XPS binding energy spectrum of Ti 2p in Fig. 2 (b) was composed of three peaks. The two main peaks were assigned to Ti $2p_{3/2}$ at the binding energy of 456.3 eV and Ti $2p_{1/2}$ at about 462 eV binding energy with spin orbital coupling of 5.6 eV. The third peak corresponds to the satellite peak [37]. After deconvoluting the high resolution XPS spectrum for O 1s in Fig. 2 (c), three peaks were exhibited at the binding energies of 530.9 eV, 529.6, and 527.7 eV. The peak at 527.7 eV corresponded to the oxygen (O^{2-}) in the TiO_2 lattice and the other O1s peak located at 529.6 eV was attributed to the formation of Ti–O–Fe bonds by substitution of Ti^{4+} with Fe^{3+} in TiO_2 lattice [38]. A large peak is found at 530.9 eV and this might belong to O^{2-} and/or O^{-} due to the formation of Na_2O and $Na_{2-x}O_x$ at the surface of the TiO_2 lattice. The deconvolution of the broad peak in the range of 682–692 eV indicates that the F is combined not only with Ti atoms exiting in the surface, but also with different links as shown in Fig. 2 (d) such as metal fluoride (Na_3TiF_6 located at 684.1 eV, $NaFeF_3$ at 685.77 eV, and Na_3FeF_6 located at 685.77 eV), partial and/or total oxygen sites substituted ($Ti_{1-y}Fe_yO_{2-x}F_x$ located at around 690.2 eV, and TiF_2 at 691.5 eV). The high resolution XPS spectrum of Fe 2p shown in Fig. 2 (e) exhibited two peaks at around the binding energies of 709.3 and 717.3 eV corresponding to the main and satellite energy state of Fe $2p_{3/2}$, respectively; and other two peaks at around 723.1 and 731.7 eV corresponding to the main and satellite energy state of Fe $2p_{1/2}$. These values indicate that the doped iron was in +3 state with spin orbital coupling of Fe $2p_{3/2}$ and Fe $2p_{1/2}$ around 13.8 eV. As presented in Fig. 2 (f), the XPS signal of Na 1s was recorded between 1060 and 1080 eV. The peaks with the binding energy of 1065.73, 1067.84, 1069.52, 1070.99, and 1072.46 eV corresponded to total and/or partial links with iron fluoride, fluorine, titanium fluoride, and oxygen (Na3FeF6, NaFeF3, NaF, Na3TiF6, and Na2O), respectively.

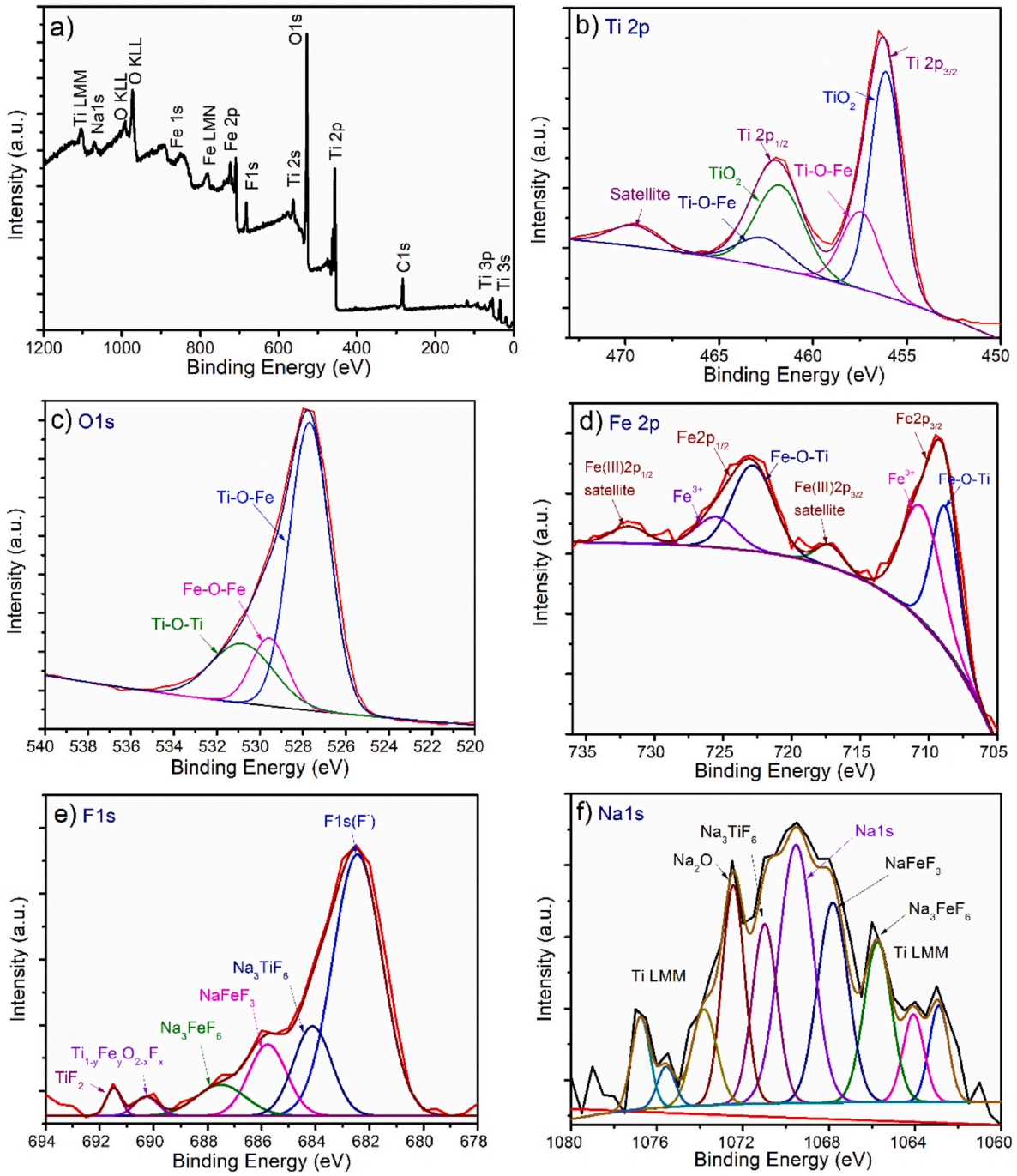

Fig. 2. XPS survey spectrum and high resolution XPS spectra of NaF25-Fe25TiO_2 nanocomposites prepared at 180 °C: a) survey spectrum; b) Ti 2p; c) O 1s; d) F 1s; e) Fe 2p; f) Na 1s.

The elemental composition of the prepared nanocomposites of NaF25-Fe25TiO_2 showed that there was no presence of any impurities. However, the weight percentage composition of Na and F as indicated in Table 2 are small in comparison to the initial moles used to synthesize the prepared nanocomposites. This is because of the large ionic radius of sodium Na^+ (around 0.102 nm) which might not substitute Ti^{4+} with radius around 0.068 nm and the high electronegativity of F which cannot totally replace oxygen. Moreover, the poor solubility of NaF in water caused the low abundance of Na and F in the synthesized nanocomposites [39].

The XPS survey in Fig. 2: a) illustrate that of NaF25-Fe25TiO_2 nanocomposite was constituted by Na, F, Ti, O, Fe and C which was due to the coating process. It should be noted that no ather elements were

Table 2
Elemental composition of the prepared Fe25% doped TiO_2 nanocomposite in the presence of 25% of NaF.

	Atomic conc. [%]	Error [%]	Mass conc. [%]	Error [%]
Ti 2p	12.33	0.25	23.27	0.47
O 1s	46.97	0.79	29.62	0.57
F 1s	4.34	0.44	3.25	0.33
Fe 2p	14.90	0.53	32.80	0.93
Na 1s	2.11	1.05	1.91	0.95
C 1s	19.35	0.71	9.16	0.38

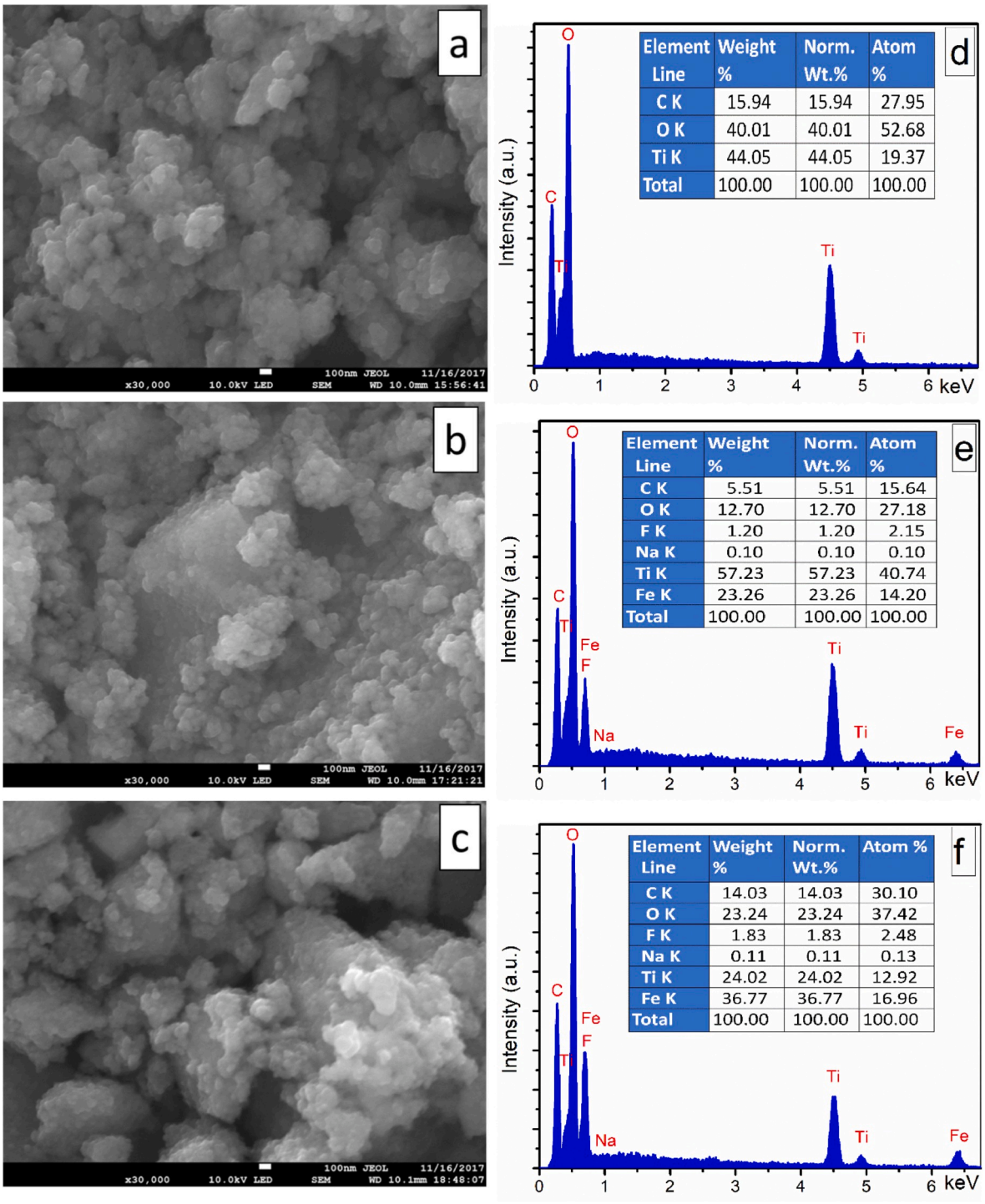

Fig. 3. a), b) and c) are HR-SEM images; d), e) and f) are EDS analysis of TiO_2, NaF10-Fe25TiO_2, and NaF25-Fe25TiO_2.

detected by SPX analysis.

3.3. Field Emission Scanning Electron Microscope (FE-SEM)/energy dispersive spectroscopy (EDS) analysis

The FE-SEM images and EDS elemental analysis of synthesized nanocomposites (i.e., TiO_2, NaF10-Fe25TiO_2, and NaF25-Fe25TiO_2) are shown in Fig. 3. The shape of TiO_2 nanoparticles was found to be clustered with homogenous and smooth structures to some extent.

The SEM images also gave an estimation of particle size diameters less than 30 nm. Moreover, the HR-SEM images showed uniform morphologies and structures in the different samples. The uniform morphologies indicate that the nano-sized TiO_2 materials have been successfully doped; thus, no deposition of any metal and/or metal oxide appears. Furthermore, TiO_2 morphologies were kept unchanged after doping TiO_2 and the diameters of the doped TiO_2 possessed almost the same average sizes as pure TiO_2.

The EDS analysis indicated that Ti, Fe, O, F, and Na were present in the prepared nanocomposites as shown in Fig. 3b) and c). The presence of the carbon peak in the EDS elemental composition was due to the

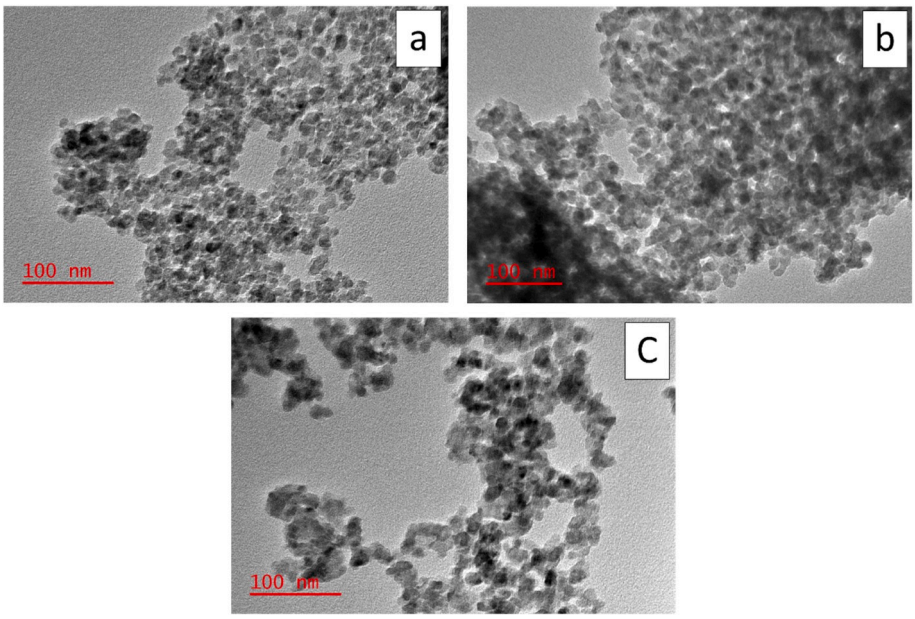

Fig. 4. a), b) and c) are TEM images of TiO_2, NaF10-Fe25TiO_2, and NaF25-Fe25TiO_2.

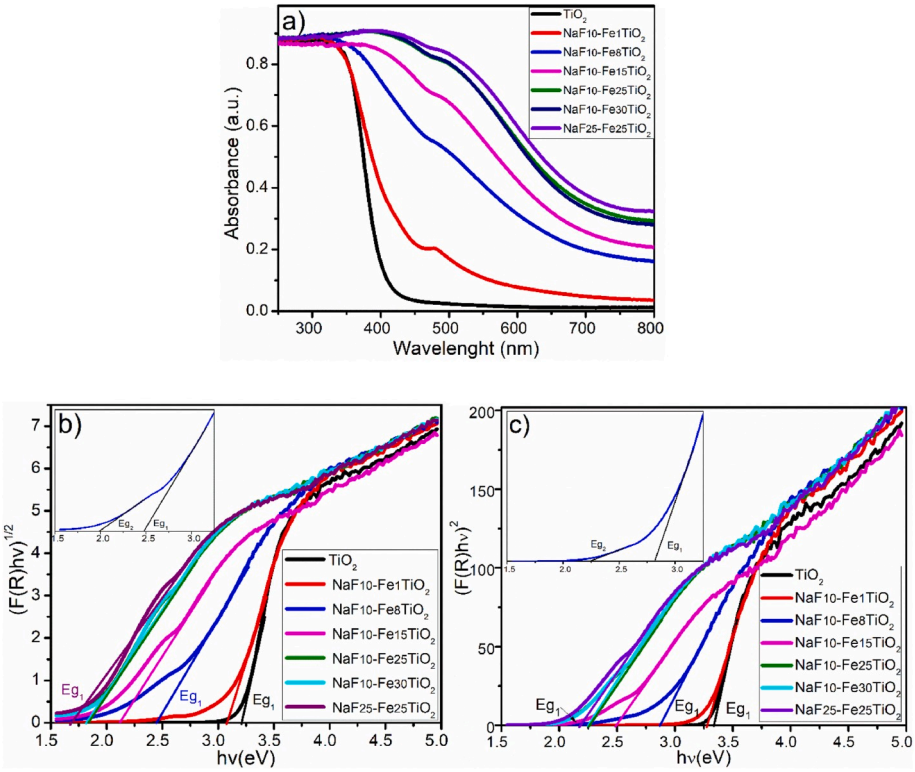

Fig. 5. (a) UV–Vis spectra, (b) indirect and (c) direct band gap of different photocatalysts based TiO_2; the band gap is achieved by substituting α by F(R) in Tauc equation and extrapolation of the straight-line part of the Tauc plot $((F(R)h\nu)^{1/2}$ and $(F(R)h\nu)^{2}$ against hν for both cases n = 2 and ½ respectively), respectively; thus, the intersection with the photon energy (hν) axes displays the band gap of the nanocomposites.

coating process with carbon. The low weight percentage of sodium (around 0.1%) and fluorine (ranging from 1.2 to 1.8%) was due to the poor solubility of NaF in water, the ionic radius of sodium and the high electronegativity of fluorine. This is in a good agreement with the XPS results which also indicates the purity of the synthesized nanocomposites.

3.4. Transmission electron microscope (TEM) studies

TEM images of pure TiO_2, NaF10-Fe25TiO_2 and NaF25-Fe25TiO_2 are shown in Fig. 4 (a), (b), and (c), respectively. The TEM images revealed an internal morphology and more accurate measurement of particle size and morphology than HR-SEM images. The TEM images of pure TiO_2 and Fe doped TiO_2 in the presence of sodium and fluorine also revealed a cluster shape with an average nanoparticle size of 10–20 nm. Doping

TiO_2 with iron in the presence of sodium and fluorine has a small effect on the particle size compared to pure TiO_2 as revealed by TEM images. Moreover, TEM image shows in Fig. 3: b) an agglomeration of NaF10-Fe25TiO_2 nanoparticles. However, the appeared agglomeration by doping TiO_2 with iron decreased by increasing the amount of sodium and fluorine in TiO_2 lattice. In fact, increasing the amount of sodium and fluorine might initiate the diffusion of iron in the TiO_2 lattice which promotes the dispersion and then diminish the agglomeration of nanoparticles.

3.5. UV–Vis absorption and band-gap of the nanocomposites

The photocatalytic activity of TiO_2 is related to the range of its spectral response. Fig. 5 (a) shows the UV–Vis absorption spectra of undoped and doped nanocomposites synthesized at 180 °C, calcined at 400 °C in air. The pure TiO_2 nanomaterials showed an absorbance in the UV range which extended in the wavelength range of 250–400 nm. However, after doping TiO_2 with Fe, in the presence of 10% of NaF, the photocatalytic activity of TiO_2 was extended to the visible light region. Thus, by increasing the amount of Fe the photocatalytic absorption increased until 25% in terms of moles, where the absorbance reached its limit.

By increasing the amount of NaF up to 25%, the photo-absorption increased again slightly. Increasing the amount of both NaF and Fe broadened the light response range of TiO_2. This slight absorbance increase was due to the new crystalline phase ($NaFeF_3$ and Na_3TiF_6). Incorporating Fe in TiO_2 and increasing the amount of NaF resulted to a red-shift of the absorbance and thereby enhanced the absorption performance in UV–Vis light region.

The generation of new phases ($NaFeF_3$ and Na_3TiF_6) in the TiO_2 based nanocomposite matrix, by increase the amount of NaF and F during the preparation, lead to an indirect or direct transition band gap. Indeed, the entire band bap of the prepared nanocomposites is estimated using Tauc equation for both permitted indirect transition and permitted direct transition in order to study the possible cases.

3.5.1. Band gap of the nanocomposite for permitted indirect transition

The band gap of the pristine TiO_2 and TiO_2 based nanocomposites for the permitted indirect transition (for n = 2 in Tauc equation) are shown in Fig. 5 (b). By extrapolating the straight-line part of the Tauc plot $((F(R)h\nu)^{1/2}$ against $h\nu)$, the optical band gap of the TiO_2 nanocomposites could be estimated from the intersection of the extrapolated straight lines and the photon energy ($h\nu$) axes. The pristine TiO_2 shows a single indirect band gap Eg, while the TiO_2 based nanocomposites prepared display tow indirect band gaps Eg_1 and Eg_2.

In the case of pure TiO_2, the primary band gap was determined to be Eg = 3.21 eV, which was attributed to a mixture of TiO_2 anatase and brookite phases with an indirect band gap Eg = 3.2 eV and Eg = 3.4 eV respectively, as mentioned in literature. However, a significant narrowing of the indirect band gap to approximately Eg_1 = 1.67 eV and Eg_2 = 1.83 eV, caused by doping TiO_2 with 25% of Fe in the presence of 25% of NaF, was observed. This broad indirect band gap shift, from Eg = 3.21 eV to Eg_1 = 1.67 eV and Eg_2 = 1.83 eV, promote the extension of an efficient photocatalytic absorption to the visible light region.

The indirect band gap of the TiO_2 nanocomposites has been narrowed and shifted first from Eg = 3.21 eV to Eg_1 = 3.08 eV and Eg_2 = 2.37 eV by introducing 1% of Fe in the presence of 10% of NaF, in terms of moles. This further indirect band daps decrease, from Eg_1 = 3.08 eV to Eg_1 = 1.81 eV and Eg_2 = 2.37 eV to Eg_2 = 1.86 eV, by increasing the amount of Fe up to 25% in the presence of 10% of NaF where the indirect band gap kept almost same value despite increasing the amount Fe. However, by increasing the amount of NaF to 25% the indirect band gap decreased again from Eg_1 = 1.81 eV and Eg_2 = 1.86 eV to Eg_1 = 1.67 eV and Eg_2 = 1.83 eV. This indirect band gap reduction between NaF10-Fe25TiO_2 and NaF_{25}-$Fe_{25}TiO_2$ was caused by the formation of $NaFeF_3$ and Na_3TiF_6 phases after increasing the amount of NaF to 25% in terms of moles.

Table 3
Indirect and direct band gaps of TiO_2 undoped and Fe doped TiO_2 in the presence of NaF.

Nanocomposite	Indirect band gap		Direct band gap	
	Eg1 (eV)	Eg2 (eV)	Eg1 (eV)	Eg2 (eV)
TiO_2	3.21	_	3.34	_
NaF10-Fe1TiO_2	3.08	2.37	3.28	_
NaF10-Fe8TiO_2	2.45	1.97	2.87	2.25
NaF10-Fe15TiO_2	2.12	1.93	2.49	2.13
NaF10-Fe25TiO_2	1.81	1.86	2.26	2.09
NaF10-Fe30TiO_2	1.84	1.87	2.25	2.10
NaF25-Fe25TiO_2	1.67	1.83	2.17	2.05

3.5.2. Band gap of the nanocomposite for permitted direct transition

The band gap of the pristine TiO_2 and TiO_2 based nanocomposites in case of permitted direct transition materials (for n = ½ in Tauc equation) are shown in Fig. 5 (c). To evaluate the direct band gaps of TiO_2 based nanocomposites the intersections of the extrapolated straight lines of the Tauc plot ($(F(R)h\nu)^2$ against $h\nu$) with the energy ($h\nu$) axis were studied (Fig. 5 (c)). Direct band gaps of TiO_2 based nanocomposites show less decrease compared to the indirect band gaps which was narrowed from Eg = 3.34 eV, attributed to the direct transitions of pristine TiO_2, to Eg_1 = 2.17 eV and Eg_2 = 2.05 eV related to the direct band gap of NaF25-Fe25TiO_2 nanocomposites. The comparison between the indirect and direct band gaps shows that Eg_1 were less than Eg_2 of the indirect band gaps while Eg_1 of the direct band gaps were higher than Eg_2.

The following Table 3 resume the indirect and direct band gaps of TiO_2 nanomaterial and TiO_2-based nanocomposites obtained from the intersection of the extrapolated straight-line part of the Tauc plot $((F(R)h\nu)^{1/2}$ and $(F(R)h\nu)^2$ against $h\nu)$, with the photon energy ($h\nu$) axes.

The origin of the enhanced visible-light absorption due to the increased amount of NaF was mainly because of the formation of additional phases that led to more energy levels which contribute to the shift and narrow of the entire optical band gap of TiO_2 based nanocomposites. Indeed, adding new energy levels which belongs to the new phases ($NaFeF_3$ and Na_3TiF_6 shown by XRD and XPS analyses) generated by increasing the amount of NaF has an effective role on the narrowing of the entire band gap of the prepared nanocomposites. Thus, NaF has an important effect on the optical properties of TiO_2 doped with Fe atoms wherein the entire band gap of the nanocomposite in decreased rendering the materials functional in various applications.

4. Conclusion

Fe-doped TiO_2 nanocomposites were successfully synthesized via a facile microwave assisted hydrothermal synthesis method. Doping TiO_2 with Fe in the presence of Na and F had a significant effect in the extension of the photocatalytic absorption of TiO_2 to the visible region. The presence of NaF converted the brookite-anatase phases to anatase-rutile phases. Na showed a strong competition against F by favoring the growth of higher percentage of rutile than the anatase phase. Moreover, because of the large ionic radius of Na and the high electronegativity of F, these ions acted as control agents for the growth of anatase and rutile phases but not as dopants. Doping TiO_2 with Fe extended the photocatalytic activity to the visible region by adding new energy levels (Fe 2p with spin orbit of 1/2 and Fe 2p with spin orbit of 2/3) between the valence and the conductive bands of TiO_2 band gap. The Fe-doped TiO_2 nanocomposites were found to exhibit higher absorption of the visible light by increasing the amount of NaF due to the formation of new crystalline phases such as Na_3TiF_6, $NaFeF_3$ and Na_3FeF_6. This simple and efficient strategy to control the growth of both anatase and rutile phases and enhance the photocatalytic activity of Fe-doped TiO_2 by introducing NaF offers a real opportunity for other elements as

dopants to reinforce the photocatalytic activity of TiO_2.

Declaration of competing interest

The authors declare that they have no known competing financial interests or personal relationships that could have appeared to influence the work reported in this paper.

CRediT authorship contribution statement

Majid Jahdi: Writing - original draft, Data curation. **Shivani B. Mishra:** Conceptualization, Funding acquisition, Project administration, Resources, Supervision. **Edward N. Nxumalo:** Supervision, Writing - review & editing. **Sabelo D. Mhlanga:** Supervision, Writing - review & editing. **Ajay K. Mishra:** Conceptualization, Funding acquisition, Project administration, Resources, Supervision, Writing - review & editing.

Acknowledgement

This work was supported by the University of South Africa (Nanotechnology and Water Sustainability Research Unit), the National Research Foundation (NRF), and the Water Research Commission (WRC).

References

[1] A. Fujishima, X. Zhang, D.A. Tryk, TiO_2 photocatalysis and related surface phenomena, Surf. Sci. Rep. 63 (2008) 515–582, https://doi.org/10.1016/j.surfrep.2008.10.001.

[2] W.Q. Li, X. Liu, H.X. Li, Hydrothermal synthesis of graphene/Fe^{3+}-doped TiO_2 nanowire composites with highly enhanced photocatalytic activity under visible light irradiation, J. Mater. Chem. A. 3 (2015) 15214–15224, https://doi.org/10.1039/c5ta00763a.

[3] W. Hu, L. Li, G. Li, C. Tang, L. Sun, High-quality brookite TiO_2 flowers: synthesis, characterization, and dielectric performance, Cryst. Growth Des. 9 (2009) 3676–3682, doi:doi.org/10.1021/cg9004032.

[4] T.-J. Whang, H.-Y. Huang, M.-T. Hsieh, J.-J. Chen, Laser-Induced silver nanoparticles on titanium oxide for photocatalytic degradation of methylene blue, Int. J. Mol. Sci. 10 (2009) 4707–4718, https://doi.org/10.3390/ijms10114707.

[5] M. Kapilashrami, Y. Zhang, Y.-S. Liu, A. Hagfeldt, J. Guo, Probing the optical property and electronic structure of TiO_2 nanomaterials for renewable energy applications, Chem. Rev. 114 (2014) 9662–9707, https://doi.org/10.1021/cr5000893.

[6] S. Li, C. Du, D. Zhao, H. Liu, Y. Wang, Synthesis of three-dimensional ordered macroporous TiO_2, Gd/TiO_2 and their photocatalytic activity, J. Porous Mater. 21 (2014) 939–945, https://doi.org/10.1007/s10934-014-9842-3.

[7] H. Khan, I.K. Swati, Fe^{3+}-doped anatase TiO_2 with d-d transition, oxygen vacancies and Ti^{3+} centers: synthesis, characterization, UV-vis photocatalytic and mechanistic studies, Ind. Eng. Chem. Res. 55 (2016) 6619–6633, https://doi.org/10.1021/acs.iecr.6b01104.

[8] Z. Zhang, M.F. Hossain, T. Takahashi, Self-assembled hematite (α-Fe_2O_3) nanotube arrays for photoelectrocatalytic degradation of azo dye under simulated solar light irradiation, Appl. Catal. B Environ. 95 (2010) 423–429, https://doi.org/10.1016/j.apcatb.2010.01.022.

[9] J. Zhu, F. Chen, J. Zhang, H. Chen, M. Anpo, Fe^{3+}-TiO_2photocatalysts prepared by combining sol-gel method with hydrothermal treatment and their characterization, J. Photochem. Photobiol. A Chem. 180 (2006) 196–204, https://doi.org/10.1016/j.jphotochem.2005.10.017.

[10] Q. He, Z. Zhang, J. Xiong, Y. Xiong, H. Xiao, A novel biomaterial - Fe_3O_4:TiO_2 core-shell nano particle with magnetic performance and high visible light photocatalytic activity, Opt. Mater. (Amst). 31 (2008) 380–384, https://doi.org/10.1016/j.optmat.2008.05.011.

[11] T. Xin, M. Ma, H. Zhang, J. Gu, S. Wang, M. Liu, Q. Zhang, A facile approach for the synthesis of magnetic separable Fe_3O_4@TiO_2, core-shell nanocomposites as highly recyclable photocatalysts, Appl. Surf. Sci. 288 (2014) 51–59, https://doi.org/10.1016/j.apsusc.2013.09.108.

[12] A.M. Czoska, S. Livraghi, M. Chiesa, E. Giamello, S. Agnoli, G. Granozzi, E. Finazzi, C. Di Valentiny, G. Pacchioni, The nature of defects in fluorine-doped TiO_2, J. Phys. Chem. C 112 (2008) 8951–8956, https://doi.org/10.1021/jp8004184.

[13] T. Butburee, K. Faungnawakij, W. Thongsuwan, W. Sangkhun, Q. Tang, H. Wang, P. Kotchasarn, Z. Sun, P. Kumnorkaew, P. Hirunsit, P. Khemthong, New understanding of crystal control and facet selectivity of titanium dioxide ruling photocatalytic performance, J. Mater. Chem. A. 7 (2019) 8156–8166, https://doi.org/10.1039/c8ta11475g.

[14] D.A.H. Hanaor, C.C. Sorrell, Review of the anatase to rutile phase transformation, J. Mater. Sci. 46 (2011) 855–874, https://doi.org/10.1007/s10853-010-5113-0.

[15] S. Shalini, N. Prabavathy, R. Balasundaraprabhu, T. Satish Kumar, P. Walke, S. Prasanna, D. Velayuthapillai, Effect of Na doping on structure, morphology and properties of hydrothermally grown one dimensional TiO_2 nanorod structures, J. Mater. Sci. Mater. Electron. 28 (2017) 3500–3508, https://doi.org/10.1007/s10854-016-5949-4.

[16] I. Singh, B. Birajdar, Synthesis, characterization and photocatalytic activity of mesoporous Na-doped TiO_2 nano-powder prepared *via* a solvent-controlled non-aqueous sol–gel route, RSC Adv. 7 (2017) 54053–54062, https://doi.org/10.1039/C7RA10108B.

[17] S. Sood, A. Umar, S.K. Mehta, S.K. Kansal, Highly effective Fe-doped TiO_2 nanoparticles photocatalysts for visible-light driven photocatalytic degradation of toxic organic compounds, J. Colloid Interface Sci. 450 (2015) 213–223, https://doi.org/10.1016/j.jcis.2015.03.018.

[18] Y. Dong, M. Kapilashrami, Y. Zhang, J. Guo, Morphology change and band gap narrowing of hierarchical TiO_2 nanostructures induced by fluorine doping, CrystEngComm 15 (2013), 10657, https://doi.org/10.1039/c3ce41390j.

[19] Y. Liu, X. Chen, Q. Ma, An Efficient Microwave-Assisted Hydrothermal Synthesis of High-Quality CuInZnS/ZnS Quantum Dots, 2018, pp. 4102–4108, https://doi.org/10.1039/c7nj05062c.

[20] B.I. Kharisov, R. Schmidt, Microwaves: microwave-assisted hydrothermal synthesis of nanoparticles, CRC Concise Encycl. Nanotechnol (2018) 585–596, https://doi.org/10.1201/b19457-49.

[21] M. Jahdi, S.B. Mishra, E.N. Nxumalo, S.D. Mhlanga, A.K. Mishra, Smart pathways for the photocatalytic degradation of sulfamethoxazole drug using F-Pd co-doped TiO_2 nanocomposites, Appl. Catal. B Environ. 267 (2020), 118716, https://doi.org/10.1016/j.apcatb.2020.118716.

[22] L. Cui, K.N. Hui, K.S. Hui, S.K. Lee, W. Zhou, Z.P. Wan, C.H. Thuc, Facile microwave-assisted hydrothermal synthesis of TiO_2 nanotubes, Mater. Lett. 75 (2012) 175–178, https://doi.org/10.1016/j.matlet.2012.02.004.

[23] Z. Zhang, O. Bondarchuk, B.D. Kay, J.M. White, Z. Dohnálek, Direct visualization of 2-butanol adsorption and dissociation on TiO_2 (110), J. Phys. Chem. C 111 (2007) 3021–3027, https://doi.org/10.1021/jp067461c.

[24] Z. Xin, L. Li, X. Zhang, W. Zhang, Microwave-assisted hydrothermal synthesis of chrysanthemum-like Ag/ZnO prismatic nanorods and their photocatalytic properties with multiple modes for dye degradation and hydrogen production, RSC Adv. 8 (2018) 6027–6038, https://doi.org/10.1039/c7ra12097d.

[25] J. Tauc, A. Menth, States in the gap, J. Non-Cryst. Solids 8–10 (1972) 569–585, https://doi.org/10.1016/0022-3093(72)90194-9.

[26] P. Ganguly, S. Mathew, L. Clarizia, S. Kumar R, A. Akande, S. Hinder, A. Breen, S. C. Pillai, Theoretical and experimental investigation of visible light responsive $AgBiS_2$-TiO_2 heterojunctions for enhanced photocatalytic applications, Appl. Catal. B Environ. 253 (2019) 401–418, https://doi.org/10.1016/j.apcatb.2019.04.033.

[27] M.D. Dramićanin, Z. Antić, S. Ćulubrk, S.P. Ahrenkiel, J.M. Nedeljković, Self-referenced luminescence thermometry with Sm^{3+} doped TiO_2 nanoparticles, Nanotechnology 25 (2014), 485501, https://doi.org/10.1088/0957-4484/25/48/485501.

[28] W. Kang, C.S. Spanjers, R.M. Rioux, J.D. Hoefelmeyer, Synthesis of brookite TiO_2 nanorods with isolated Co(II) surface sites and photocatalytic degradation of 5,8-dihydroxy-1,4-naphthoquinone dye, J. Mater. Chem. A. 1 (2013) 7717–7728, https://doi.org/10.1039/c3ta11038a.

[29] S. Kumar, B. Kishore, N. Munichandraiah, Electrochemical studies of non-aqueous Na-O_2 cells employing Ag-RGO as the bifunctional catalyst, RSC Adv. 6 (2016) 63477–63479, https://doi.org/10.1039/c6ra13596j.

[30] K. He, F.X. Ma, C.Y. Xu, J. Cumings, Mapping magnetic fields of Fe_3O_4 nanosphere assemblies by electron holography, J. Appl. Phys. 113 (2013) 1–4, https://doi.org/10.1063/1.4798500.

[31] X. Zhang, Y. Niu, X. Meng, Y. Li, J. Zhao, Structural evolution and characteristics of the phase transformations between α-Fe_2O_3, Fe_3O_4 and γ-Fe_2O_3 nanoparticles under reducing and oxidizing atmospheres, CrystEngComm 15 (2013) 8166–8172, https://doi.org/10.1039/c3ce41269e.

[32] X. Gu, N. Yu, L. Zhang, J. Yang, J. Hu, Z. Chen, Growth of TiO_2 nanorod bundles on carbon fibers as flexible and weaveable photocatalyst/photoelectrode, RSC Adv. 5 (2015) 102868–102876, https://doi.org/10.1039/c5ra21344d.

[33] L. Zhu, Q. Lu, L. Lv, Y. Wang, Y. Hu, Z. Deng, Z. Lou, Y. Hou, F. Teng, Ligand-free rutile and anatase TiO_2 nanocrystals as electron extraction layers for high performance inverted polymer solar cells, RSC Adv. 7 (2017) 20084–20092, https://doi.org/10.1039/c7ra00134g.

[34] S. Wang, X. Liu, L. Wang, Q. Wen, N. Du, J. Huang, Formation mechanism and properties of fluoride-phosphate conversion coating on titanium alloy, RSC Adv. 7 (2017) 16078–16086, https://doi.org/10.1039/c6ra27199e.

[35] K.V. Kravchyk, T. Zünd, M. Wörle, M.V. Kovalenko, M.I. Bodnarchuk, $NaFeF_3$ nanoplates as low-cost sodium and lithium cathode materials for stationary energy storage, Chem. Mater. 30 (2018) 1825–1829, https://doi.org/10.1021/acs.chemmater.7b04743.

[36] N. McElroy, R.C. Page, D. Espinbarro-Valazquez, E. Lewis, S. Haigh, P. O'Brien, D. J. Binks, Comparison of solar cells sensitised by CdTe/CdSe and CdSe/CdTe core/shell colloidal quantum dots with and without a CdS outer layer, Thin Solid Films 560 (2014) 65–70, https://doi.org/10.1016/j.tsf.2013.10.085.

[37] M.H. Pham, C.T. Dinh, G.T. Vuong, N.D. Ta, T.O. Do, Visible light induced hydrogen generation using a hollow photocatalyst with two cocatalysts separated on two surface sides, Phys. Chem. Chem. Phys. 16 (2014) 5937–5941, https://doi.org/10.1039/c3cp54629b.

[38] G.K. Alqurashi, A. Al-Shehri, K. Narasimharao, Effect of TiO2 morphology on the benzyl alcohol oxidation activity of Fe_2O_3-TiO_2 nanomaterials, RSC Adv. 6 (2016) 71076–71091, https://doi.org/10.1039/c6ra13958b.

[39] J.G. Reynolds, J.D. Belsher, A review of sodium fluoride solubility in water, J. Chem. Eng. Data 62 (2017) 1743–1748, https://doi.org/10.1021/acs.jced.7b00089.